Power line harmonic radiation observed by satellite: Properties and propagation through the ionosphere

F. Němec, O. Santolík, Michel Parrot, J. Bortnik

Power line harmonic radiation observed by satellite: Properties and propagation through the ionosphere

F. Němec,[1,2,3] O. Santolík,[2,3] M. Parrot,[1] and J. Bortnik[4]

Received 19 March 2008; revised 25 April 2008; accepted 2 May 2008; published 27 August 2008.

[1] We present results of a systematic survey of power line harmonic radiation events observed by the low-altitude DEMETER spacecraft. Altogether, 88 events (45 with frequency spacing 50/100 Hz and 43 with frequency spacing 60/120 Hz) have been found by an automatic identification procedure and confirmed by visual inspection. Frequency-Time intervals of individual lines forming the events have been found by an automated procedure, and the corresponding frequency-time spectrograms have been fitted by a 2d-Gaussian model. It is shown that the mean time duration of the lines forming the events is 20 seconds, with median being 12 seconds (this corresponds to the spatial dimensions of 156/90 km, respectively). The full width at half maximum of the frequency range of the lines is less than 3 Hz in the majority of cases. Moreover, the lines with larger bandwidth and the lines with the largest intensities often occur off exact multiples of base power system frequency. This can be explained either by wave-particle interactions that take place and modify the radiated electromagnetic wave or by the improperly operating radiating power system. Full-wave calculation of the efficiency of coupling of electromagnetic waves through the ionosphere has been done to show that it can explain lower intensity of events observed by satellite during the day as compared with those observed during the night. Estimated radiated peak power on the ground is larger for events observed during the day than for events observed during the night, and more events are observed during the day than during the night.

Citation: Němec, F., O. Santolík, M. Parrot, and J. Bortnik (2008), Power line harmonic radiation observed by satellite: Properties and propagation through the ionosphere, *J. Geophys. Res.*, *113*, A08317, doi:10.1029/2008JA013184.

1. Introduction

[2] Power line harmonic radiation (PLHR) are electromagnetic waves radiated by electric power systems on the ground at harmonic frequencies of 50 or 60 Hz, depending on the frequency of the system. When represented in the form of frequency-time spectrograms, they usually have a form of intense parallel lines with mutual distances of 50/100 or 60/120 Hz, because odd/even harmonics can sometimes be strongly suppressed. Such emissions are often observed on the ground and evidence for their propagation through the magnetosphere has been shown [*Helliwell et al.*, 1975; *Park and Helliwell*, 1978; *Matthews and Yearby*, 1981; *Park and Helliwell*, 1981; *Park and Helliwell*, 1983; *Yearby et al.*, 1983; *Manninen*, 2005]. However, direct observations by satellites are rather rare and with a few exceptions [*Rodger et al.*, 1995; *Němec et al.*, 2006, 2007b] these studies usually reported only a low number of events [*Koons et al.*, 1978; *Bell et al.*, 1982; *Tomizawa and Yoshino*, 1985; *Parrot et al.*, 2005].

[3] *Rodger et al.* [1995] performed the first satellite survey with a significant number of included events and reported the existence of two distinct classes of events: the first of them (''Tram Lines'', TL) consisted of events that appeared to lie close to the harmonics of 50/60 Hz; the second class of events (''Magnetospheric Line Radiation'', MLR), formed by lines with larger bandwidth, did not show any evidence of a relationship with power line harmonics. *Němec et al.* [2007a] performed a systematic survey of MLR-like events using the data from DEMETER spacecraft. They confirmed the existence of the two classes of events (PLHR and ''real-MLR'') and demonstrated their different properties (intensity, frequency, most favorable values of Kp index).

[4] *Němec et al.* [2006] analyzed DEMETER observations of PLHR events and showed that the frequency spacing of the lines corresponds well to the power system frequency in possible generation regions. Moreover, they have shown that the peak intensity of PLHR is larger during the night than during the day, suggesting different penetration characteristics of the ionosphere as a possible explanation. *Ando et al.* [2002] performed a theoretical analysis of

[1]Laboratoire de Physique et Chimie de l'Environnement/CNRS, Orléans, France.
[2]Faculty of Mathematics and Physics, Charles University, Prague, Czech Republic.
[3]Institute of Atmospheric Physics, Academy of Sciences of the Czech Republic, Prague, Czech Republic.
[4]Department of Atmospheric and Oceanic Sciences, University of California Los Angeles, Los Angeles, California, USA.

0148-0227/08/2008JA013184

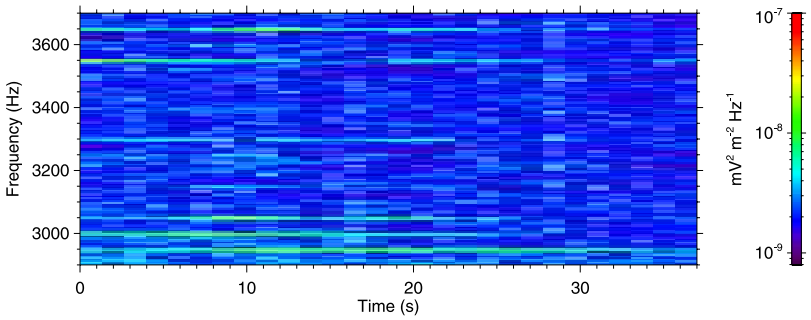

Figure 1. An example of frequency-time spectrogram of power spectral density of electric field fluctuations corresponding to one of the identified events. The data were recorded on 21 September 2006 between 10:06:02 and 10:06:39 UT. The lines occur at exact multiples of 50 Hz.

penetration of PLHR into the ionosphere and estimated the horizontal size of the region where the electromagnetic field is strong to about ±200 km from the source, not extending with higher altitude.

[5] *Park and Miller* [1979] reported the existence of "Sunday effect" – they claimed that the wave activity during Sundays was lower that the wave activity during the weekdays, attributing this difference to a lower power consumption. *Parrot et al.* [1991] and *Molchanov et al.* [1991] confirmed the existence of this effect and argued that it can be caused not only by a lower power consumption during the weekends as compared to the weekdays, but also by a different current distribution in power systems. However, other authors who searched for the existence of the effect [*Rodger et al.*, 2000; *Karinen et al.*, 2002] concluded that it is only a statistical fluctuation. The role of PLHR in the ionosphere and magnetosphere is thus still questionable, but it could be quite important, because they can serve as a trigger for naturally generated whistler-mode emissions [*Nunn et al.*, 1999; *Manninen*, 2005]. Moreover, they can be also important for electron precipitation [*Bullough*, 1995].

[6] Observations of PLHR events, some of their properties and numerical calculation of their penetration through the ionosphere up to the DEMETER altitude are reported in this paper. The wave experiment on board DEMETER is briefly introduced in section 2. An automatic procedure for identification of PLHR events and frequency-time-dependent 2d-Gaussian model of individual lines that are forming the events are described in section 3. Section 4 describes some of the properties of the observed events, whereas section 5 presents a calculation of penetration characteristics of PLHR through the ionosphere. The obtained results are discussed in section 6 and summarized in section 7.

2. Experiment

[7] We have used wave measurements from the French micro-satellite DEMETER (altitude 700 km, inclination 98 degrees, nearly Sun-synchronous orbit, mass 130 kg, launched in June 2004). [*Berthelier et al.*, 2006; *Parrot et al.*, 2006; *Santolík et al.*, 2006]. The scientific instruments placed on board DEMETER record data during the entire orbit with an exception of geomagnetic latitudes larger than 65 degrees. Because of the limited capacity of the telemetry, there are two different modes of operation. A "Survey mode" measuring low-resolution data provides us in VLF range (up to 20 kHz) with power spectra of one electric and one magnetic field component. However, the limited frequency resolution (19.53 Hz) is not sufficient for our study – both the identification of events and their subsequent analysis require frequency resolution better than 5 Hz. We have consequently used the "Burst mode", which is active only above some specific areas of interest, but provides us with waveforms of one electric and one magnetic field component (at a sampling frequency of 40 kHz).

3. Automatic Identification of Events

[8] The data set that we have used is too large to be processed manually. Instead, we have used an automatic identification procedure described by *Němec et al.* [2006]. It searches the measured data for presence of possible PLHR events and provides us with their time, frequency and spectrogram of the surrounding interval in the frequency-time plane. We have then manually checked the positively identified events and we have decided whether a real event was found or a "false alarm" occurred. Within 1499 cases identified by the automatic procedure run on the entire data set of 3378 hours of Burst mode waveform data recorded between 12 August 2004 and 3 February 2008, only 88 PLHR events have been found. Among these, 45 events have the frequency spacing of 50/100 Hz and 43 events have the frequency spacing of 60/120 Hz. This represents about twice larger data set as compared to *Němec et al.* [2007b]. Their results have been well confirmed, namely the frequency spacing of the lines corresponds well to the power system frequency in generation regions.

[9] An example of one of the identified events is shown in Figure 1. It represents the frequency-time spectrogram of power spectral density of electric field fluctuations measured on 21 September 2006 between 10:06:02 and 10:06:39 UT above the southern part of Sweden. Several lines at constant frequencies can be clearly seen. They occur at exact (within the experimental error) multiples of 50 Hz, namely at frequencies: 2950 Hz, 3000 Hz, 3050 Hz, 3300 Hz, 3550 Hz and 3650 Hz.

[10] Having the manually confirmed set of PLHR events and knowing approximately their beginning and ending times and frequency ranges, we apply another procedure to identify individual lines forming the events and to find parameters of their 2d-Gaussian model in a frequency-time plane. An input of this procedure is a frequency-time spectrogram of a PLHR event. The length of a FFT segment

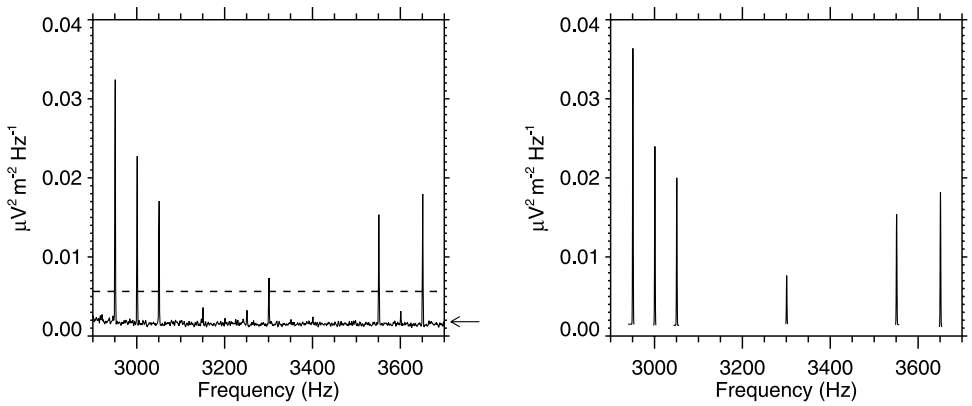

Figure 2. (left) Power spectrum corresponding to the event from Figure 1 used for the peak identification procedure. The mean value is marked by an arrow, and the minimum peak value (see text) is plotted by a dashed line. (right) Gaussian fits corresponding to the identified peaks in power spectrum.

used in the processing is 40000 points (this gives a frequency resolution of 1 Hz), overlapping is 75% and the Hanning window is used. The procedure consists of the following three steps.

[11] In the first step, peaks in the power spectrum (that is individual lines forming the events) are found and their central frequencies and widths are determined. A power spectrum that corresponds to the event presented in Figure 1 is shown in the left of Figure 2. Intense peaks located at frequencies 2950 Hz, 3000 Hz, 3050 Hz, 3300 Hz, 3550 Hz and 3650 Hz can be seen. As well as these, much weaker peaks can be observed also at frequencies 3150 Hz, 3250 Hz, 3400 Hz and 3600 Hz. The mean value of power spectral density $\bar{I}$ (marked by an arrow in the left of Figure 2) and the standard deviation σ_I of the power spectral density are calculated. Peaks are identified at frequency ranges where the power spectral density $I(f)$ is larger than a threshold value (plotted by a dashed line in the left of Figure 2)

$$I(f) > \bar{I} + \alpha\,\sigma_I \tag{1}$$

where α is a fixed constant ($\alpha = 2$). Then minimum and maximum frequencies $f^i_{\min}$ and $f^i_{\max}$ of a peak i are the closest adjacent frequencies where $I(f)$ is lower than $\bar{I}$ and reaches the local minimum. For an example case of the peak located close to 2950 Hz, these are marked by vertical lines in the Figure 3. Having found the intense peaks in power spectrum, we perform a least-squares Gaussian fit. The background intensity value ρ_i of each of the peaks is calculated as $\rho_i = (I(f^i_{\min}) + I(f^i_{\max}))/2$. This value is subtracted and the result is fitted by a Gaussian function with three free parameters: the central frequency of the peak f_i, intensity of the peak I_i and the standard deviation σ_i. The fits corresponding to the example spectrum are shown in the right of Figure 2, with frequencies f_i of the identified peaks being 2950.7 Hz, 3000.8 Hz, 3050.6 Hz, 3300.8 Hz, 3551.1 Hz and 3650.9 Hz. Figure 3 represents a detailed view of the fit performed on a peak located close to 2950 Hz. A solid line shows the measured power spectrum and the least-square Gaussian fit is over-plotted by a dashed line.

[12] The second step of the procedure consists of identification of the appropriate time intervals corresponding to individual lines which form the PLHR event. For this purpose, we calculate the time dependence of the average power spectral density in the frequency interval $(f_i - \sigma_i\sqrt{2\ln 2};\ f_i + \sigma_i\sqrt{2\ln 2})$, which is the frequency interval centered at the peak frequency of the line that has the width equal to full width of the peak at half of its maximum (FWHM). We then calculate the time-dependent "background value", which is the mean value of power spectral density in frequency intervals outside the peak, namely in intervals: $(f_i - \sigma_i\,(4 + \sqrt{2\ln 2});\ f_i - 4\,\sigma_i)$ and $(f_i + 4\,\sigma_i;\ f_i + \sigma_i\,(4 + \sqrt{2\ln 2}))$. For an example case of the peak located close to 2950 Hz, the three frequency intervals (one corresponding to the peak and two just outside of it) are marked by horizontal lines in Figure 3. This average back-

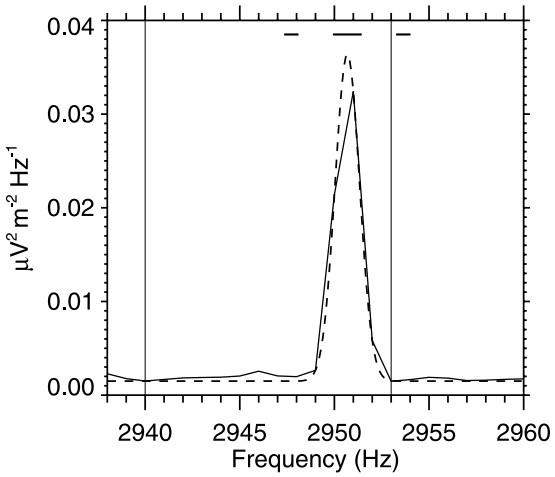

Figure 3. A detailed view of the fit performed on the peak located close to 2950 Hz. The measured power spectrum is plotted by a solid line, and the least square Gaussian fit is overplotted by a dashed line. The minimum and maximum frequencies $f^i_{\min}$ and $f^i_{\max}$ of the peak (see text) are marked by vertical lines. Horizontal lines mark the frequency intervals used in the second step of the procedure for the identification of the appropriate time interval corresponding to the line (see text).

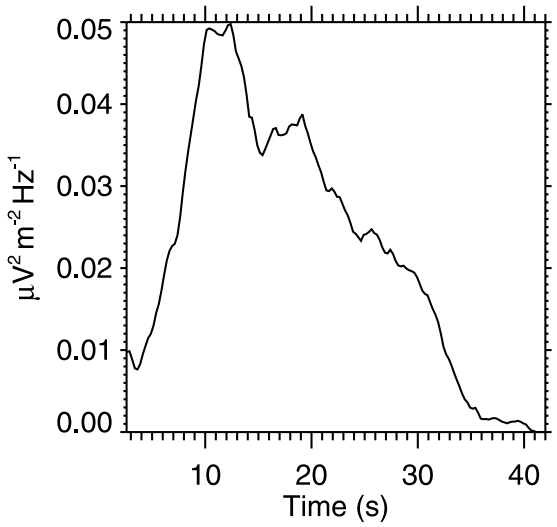

Figure 4. An example of a resulting time-dependent value of power spectral density obtained for the line located close to 2950 Hz.

ground is subtracted and a running mean over 5 seconds of data is applied. Afterwards, starting from some manually defined time when the line occurs, we span the time interval until a local minimum lower than 0 is reached on both sides. In such a way, we obtain a time interval when a given line occurs. Figure 4 shows an example of the resulting time-dependent average value of power spectral density obtained for the line located close to 2950 Hz.

[13] In the last step of the procedure a frequency-time 2d-Gaussian model is applied to the frequency-time interval corresponding to a given line:

$$I(f,t) = I_0 \exp\left(-\frac{(f-f_0)^2}{2\delta^2}\right) \exp\left(-\frac{(t-t_0)^2}{2\tau^2}\right) + I_b \quad (2)$$

The frequency interval determined in the first step, time interval determined in the second step and a moving average over 5 seconds of data are used. For each of the lines, this results in an estimate of 5 parameters: background intensity I_b, peak intensity I_0, central frequency f_0, central time t_0, characteristic time duration τ and characteristic frequency range δ. For the line considered in Figure 4, Figure 5 shows an example of its frequency-time spectrogram and its 2d-Gaussian model. All the performed fits have been visually inspected. Among 253 lines found during the first step of the procedure, 206 have been successfully fitted. In the remaining 47 cases, the fit failed, usually because of strong and varying background field intensity (typically when a whistler occurred simultaneously, being more intense than the PLHR line). Such cases have not been further used in the study.

4. Properties of the Observed PLHR Events

[14] Figure 6 represents a histogram of the FWHM of the observed time durations of individual lines forming the PLHR events (bottom scale of the x-axis) and also the same histogram but rescaled to the observed spatial dimensions (upper scale of the x-axis). The observed average FWHM of time duration is 20 seconds, with the median value of 12 seconds. This corresponds to spatial dimensions of 156 km/90 km, respectively. The difference between the mean and median values is caused by a long tail of the distribution meaning that long time durations are possible, but improbable.

[15] Figure 7 represents a histogram of FWHM of frequency ranges of individual lines forming the PLHR events. It can be seen that the frequency range of individual lines is less than 3 Hz in the majority of cases.

[16] Figure 8 represents the FWHM of the frequency range of PLHR lines as a function of peak intensity. The events with frequencies corresponding to the multiples of the power system frequency (i.e., when frequency deviation from the corresponding multiple is less than 3 Hz) are plotted by crosses, the events with frequencies not corresponding to these multiples are shown by diamonds. It can be seen that among the most intense lines, all occur off exact multiples of power system frequency. Moreover, the lines with large bandwidth occur off the exact multiples as well. This is further confirmed by Figure 9 which represents a frequency deviation from multiples of power system frequency as a function of the detected peak intensity of the events. Triangles represent lines forming the events with 50/100 Hz spacing and squares represent lines forming the events with 60/120 Hz. Similar behavior is

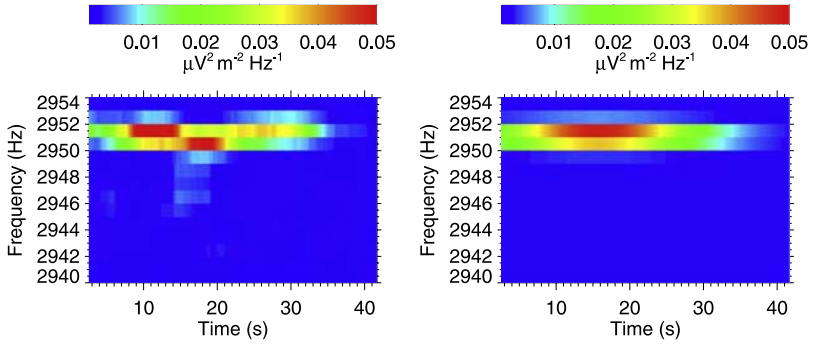

Figure 5. (left) Frequency-Time spectrogram corresponding to the line close to 2950 Hz. (right) Result of 2d-Gaussian fit.

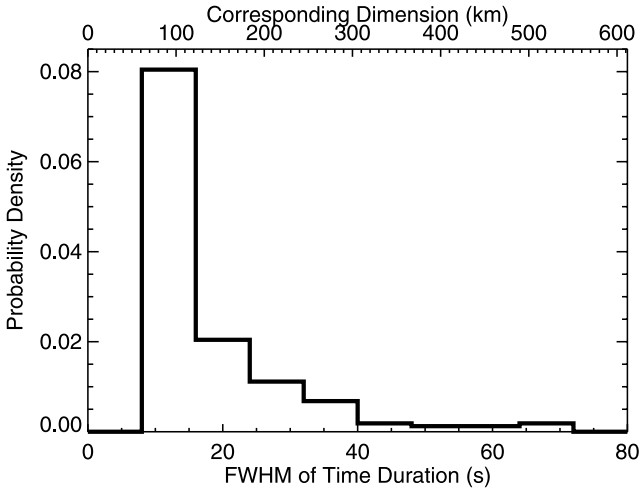

Figure 6. (Bottom scale of the x axis) Histogram of the FWHM of the time durations of the lines forming the PLHR events. (Upper scale of the x axis) Histogram of the corresponding spatial dimensions of the PLHR events.

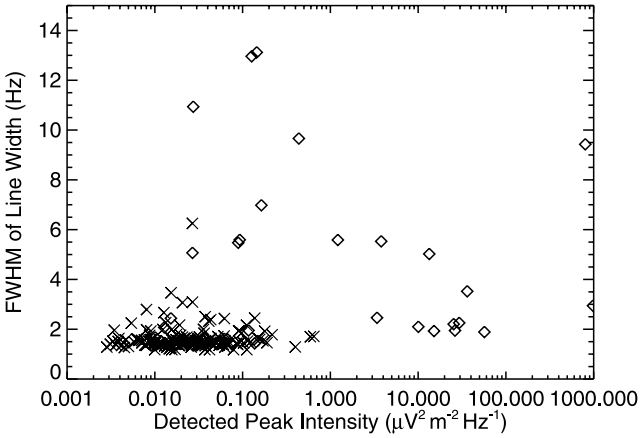

Figure 8. FWHM of frequency ranges of individual lines forming the PLHR events as a function of the peak intensity. The events with frequencies corresponding to the multiples of the power system frequency are plotted by crosses, and the events with frequencies not corresponding to these multiples are shown by diamonds.

observed for both of them. The dotted line at the frequency deviation of 3 Hz represents the chosen threshold for lines to be considered as occurring at "exact" multiple of power system frequency, as used in section 5.

5. PLHR Propagation Through the Ionosphere

[17] In the following, we consider only the lines with frequency deviation from multiples of power system frequency less than 3 Hz and generation region located just below the place of observation (not in the conjugate region) were taken into account; the events with larger deviation from multiples of power system frequency may undergo some specific interaction with the surrounding plasma environment and our calculation of the efficiency of coupling would not be consequently valid for such cases – see section 6. The left of Figure 10 represents the peak power spectral density of Poynting flux of individual lines forming the PLHR events as a function of magnetic local time. Assuming right-handed circular polarized parallel propagation [*Němec et al.*, 2006], it was calculated as

$$S = \frac{1}{2}\frac{n}{c\mu_0}E^2 \tag{3}$$

where E^2 is the peak power spectral density of electric field fluctuations of a given PLHR line, μ_0 is a permeability of vacuum, c is speed of light and n is the refractive index. The refractive index has been obtained from the cold plasma approximation, using particle concentrations from International Reference Ionosphere model [*Bilitza*, 1990] (http://modelweb.gsfc.nasa.gov/models/iri.html). Note that bunching of the observed events into two MLT intervals is

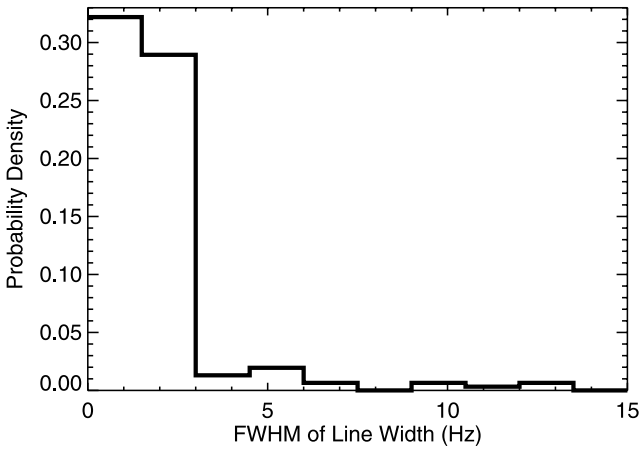

Figure 7. Histogram of the FWHM of the frequency range of the lines forming the PLHR events.

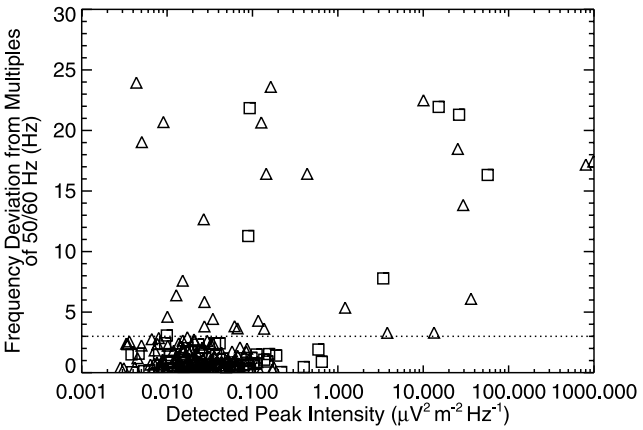

Figure 9. Frequency deviation from multiples of power system frequency as a function of the detected peak intensity. The lines forming events with frequency spacing 50/100 Hz are plotted by triangles, and the lines forming events with frequency spacing 60/120 Hz are plotted by squares.

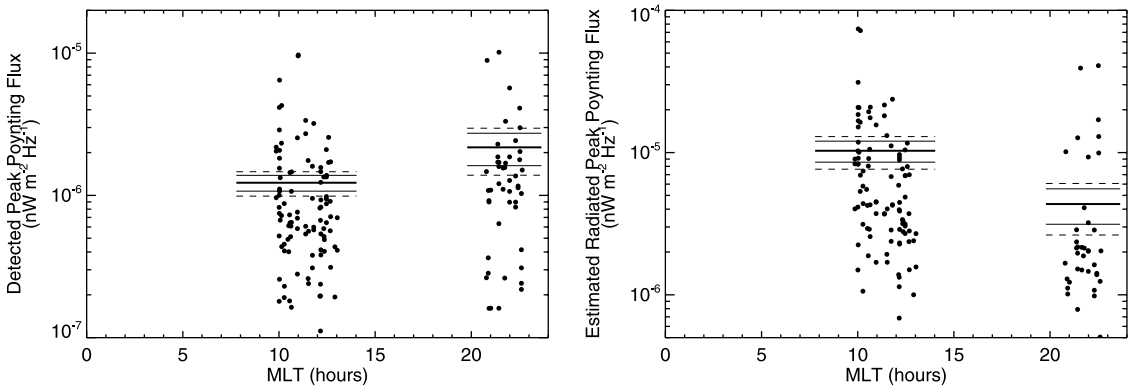

Figure 10. (left) Detected peak power spectral density of Poynting flux of individual lines forming the PLHR events as a function of the magnetic local time. The mean values for the daytime/nighttime and corresponding standard deviations (see text) are plotted by horizontal lines. (right) Estimated radiated peak power spectral density of Poynting flux of individual lines forming the PLHR events on the ground surface (calculated from the observations, taking into account the numerically calculated penetration characteristics of the ionosphere) as a function of the magnetic local time. The mean values for the daytime/nighttime and corresponding standard deviations are again marked by horizontal lines.

caused by the specific orbit of the DEMETER spacecraft. The mean peak power spectral density of Poynting flux observed during the day (43 events, 101 successfully fitted lines) is $(1.23 \pm 0.16) \cdot 10^{-6}$ nW m^{-2} Hz^{-1}. This calculation is valid if we consider individual lines as being independent, even if they form the same event (that is they are observed simultaneously, but at different frequencies). If all the lines measured within the same event were dependent, then the standard deviation would be $0.24 \cdot 10^{-6}$ nW m^{-2} Hz^{-1} instead (the standard deviation $\sigma_{\bar{x}}$ of the mean $\bar{x}$ is calculated as $\sigma_{\bar{x}} = \sigma_x/\sqrt{N_x}$ where σ_x is a standard deviation of a set x and N_x is a number of independent samples in the set x). The mean peak power spectral density of Poynting flux observed during the night (24 events, 48 successfully fitted lines altogether) is $(2.18 \pm 0.56) \cdot 10^{-6}$ nW m^{-2} Hz^{-1}, supposing the independence of the lines within the same event. For the case of completely dependent lines, the standard deviation would be $0.79 \cdot 10^{-6}$ nW m^{-2} Hz^{-1}. These values of standard deviations are marked by horizontal lines. The events observed during the night are more intense, with the difference of mean values being $(0.95 \pm 0.58) \cdot 10^{-6}$ nW m^{-2} Hz^{-1} supposing that the lines forming one event are completely independent. Supposing that the lines forming one event are completely dependent, the standard deviation increases to $0.83 \cdot 10^{-6}$ nW m^{-2} Hz^{-1}. This difference then corresponds to 1.6 and 1.1 standard deviation, respectively.

[18] *Němec et al.* [2006] suggested the efficiency of coupling through the ionosphere as a possible explanation for PLHR being more intense during the night than during the day. Here we present results of a calculation of the efficiency of coupling of electromagnetic waves through the ionosphere. The procedure of *Nagano et al.* [1975] has been followed and the full-wave code developed by *Bortnik and Bleier* [2004] has been used to obtain a full-wave solution of Maxwell's equations in the presence of electrons and several ion species. The medium is supposed to be horizontally stratified. Cold plasma approximation [*Stix*, 1992] has been used to calculate the susceptibility matrix and the effects of collisions have been included by modifying the mass of a particle m_{s0} by the collision frequency ν_s:

$$m_s = m_{s0}\left(1 - \frac{\nu_s}{\omega}\right) \tag{4}$$

To perform the calculation, the density and composition of the electron and ion populations as a function of altitude, as well as the magnetic field intensity and magnetic inclination need to be known. Moreover, it is necessary to know the collision profiles of electrons and ions since these critically control the attenuation and mode conversion.

[19] To specify electron and ion number density as a function of altitude at a given geographic location and time we have used the International Reference Ionosphere model. The collision frequency was taken from *Cummer* [2000] for the low-altitude portion of both electrons and protons (altitudes less than 300 km), where collisions with neutrals are dominant. Above this altitude, Coulomb collisions dominate and the profile from *Helliwell* [1965] has been used. Magnetic field intensity was calculated using the IGRF model at an altitude of 80 km (which is the region where most of the attenuation takes place) and was taken to be constant (though the medium is supposed to be horizontally stratified and the problem is thus effectively only 1d, we would otherwise obtain a nonphysical condition $\nabla \vec{B} \neq 0$).

[20] The efficiency of coupling of electromagnetic waves through the ionosphere is for our purposes defined as a power attenuation, that is the ratio between the final power of the wave measured on board the spacecraft and the incident power radiated from the electric power system on the ground. The calculated altitudinal dependence for two chosen geographical regions where PLHR are often observed (Finland and Japan) is plotted in Figure 11, separately for the day and the night. It can be seen that most of the attenuation takes place at altitudes of about 70–90 km (HF absorption observed by riometers is also maximum in this range of altitudes). Considering the final efficiency of

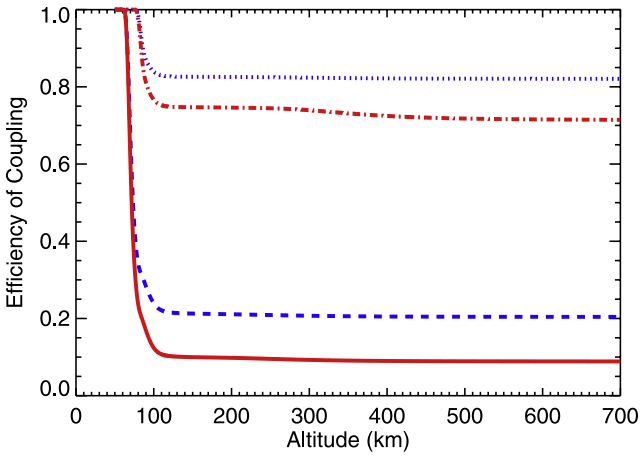

Figure 11. Efficiency of coupling for the frequency of wave 2.5 kHz as a function of the altitude for nighttime Finland region (dotted line), nighttime Japan region (dash-dotted line), daytime Finland region (dashed line), and daytime Japan region (solid line).

coupling at the altitude of DEMETER, it is about five times larger during the night (value of about 0.80, dotted and dash-dotted lines) than during the day (value of about 0.15, dashed and solid lines). Moreover, it is larger in Finland region (dotted and dashed lines) than in Japan region (dash-dotted and solid lines) – see section 6.

[21] We have calculated the efficiency of coupling of electromagnetic waves through the ionosphere for all the individual lines from the left of Figure 10. The ionospheric parameters, intensity of magnetic field and magnetic inclination were determined separately for each of them.

[22] The right of Figure 10 shows the estimated peak power spectral densities of Poynting fluxes on the ground surface that correspond to the peak power spectral densities of Poynting fluxes of individual lines measured by DEMETER, taking into account numerically calculated penetration characteristics of the ionosphere. Supposing that the individual lines are independent, the mean value of estimated peak power spectral density of Poynting flux on the ground during the day is $(1.03 \pm 0.17) \cdot 10^{-5}$ nW m^{-2} Hz^{-1}. Supposing that the lines forming one event are completely dependent, the standard deviation would be $0.27 \cdot 10^{-5}$ nW m^{-2} Hz^{-1}. The mean value of estimated peak power spectral density of Poynting flux on ground during the night is $(0.44 \pm 0.12) \cdot 10^{-5}$ nW m^{-2} Hz^{-1} and $(0.44 \pm 0.17) \cdot 10^{-5}$ nW m^{-2} Hz^{-1} for completely independent lines forming one event and completely dependent lines forming one event, respectively. The mean values and the appropriate standard deviations are again marked by horizontal lines. The estimated radiated power is therefore lower for events observed during the night, with the mean difference being $(-0.60 \pm 0.21) \cdot 10^{-5}$ nW m^{-2} Hz^{-1} and $(-0.60 \pm 0.32) \cdot 10^{-5}$ nW m^{-2} Hz^{-1} for independent/dependent lines forming one event, respectively (2.9 and 1.9 standard deviations, respectively).

6. Discussion

[23] The basic limitation of the presented study is the usage of the automatic procedure for an identification of PLHR events. This issue is discussed in detail by *Němec et al.* [2006], who used the same procedure and did not find any indication that this biases the obtained results (i.e., by the presence of a "selection effect").

[24] The recently developed procedure for an identification of individual lines forming a PLHR event described in section 3 is very simple and easy to implement. As demonstrated by Figures 2, 3, 4 and 5, it usually performs well as long as the peaks in the power spectrum are larger than the minimum peak value threshold. In about one fifth of cases (47 out of 253), the 2d-Gaussian fitting was not successful because of strong variations in the background field intensity. This principal limitation surely slightly biases the results presented in Figures 6, 7, 8, 9, 10, but the main qualitative conclusions should remain unaffected.

[25] Figure 6 shows a histogram of FWHM of the observed time durations of individual lines forming the PLHR events and corresponding spatial dimensions. Although the performed measurements (one satellite only) do not allow us to distinguish between temporal and spatial variations of the signal, it is reasonable to suppose that the electromagnetic radiation from the power systems on the ground is temporarily rather stable. Consequently, the observed time durations correspond more likely to the spatial dimensions of individual PLHR events. The average corresponding spatial dimension of 156 km (median 90 km) is in a relatively good agreement with theoretically calculated dimensions of the affected region [*Ando et al.*, 2002].

[26] Figures 8 and 9 suggest that there is a connection between the frequency deviation of individual lines forming the PLHR events from the exact harmonic multiples of power system frequency, their bandwidth and their intensity – lines with large peak intensities have also large frequency deviation from the appropriate harmonic. Moreover, the lines with large bandwidth usually occur off exact multiples of power system frequency as well. This can be caused by two different phenomena. First, while most of the PLHR events—after being radiated from an electric power system on the ground—propagate up to the satellite altitudes almost unchanged (only slightly attenuated, as shown in the numerical simulation in section 5), some of them may undergo interactions with the plasma environment, which shifts their peak frequencies (originally located close to the exact multiples of power system frequency). Such interactions can predominantly occur for events with larger observed intensity. They may be also responsible for larger bandwidth of such events. The second possible explanation is that the most intense PLHR occur due to some specific events in power systems. During these events, larger harmonics are present in the power system and its base frequency may be slightly shifted off 50/60 Hz. Afterwards, an explanation proposed by *Němec et al.* [2007b] could be used for such events: a small shift of base power system frequency off 50/60 Hz is too small to be observed in the frequency spacing between individual lines, but at higher harmonics (that are typically observed) it can lead to a significant shift in frequency. Improperly operating power systems could also explain a larger bandwidth of the observed lines. The effect of the Doppler shift does not play a significant role in the study; it causes shifts of maximally about 3 Hz, usually being much lower. Moreover, a case study performed by *Parrot et al.* [2007] has

experimentally proven that—for that particular event—the frequencies of the lines observed simultaneously by satellite and on the ground are not significantly different.

[27] The performed full-wave calculation reveals substantial variability of the efficiency of coupling of electromagnetic waves through the ionosphere. The power that penetrates up to the DEMETER altitudes is about five times less attenuated during the night than during the day. Moreover, the efficiency of coupling is larger in the Finland region as compared to the Japan region, even the difference is not so striking as the day/night asymmetry (Figure 11). This is caused by different geomagnetic latitudes of Finland (57.5°) and Japan (23°). The electromagnetic waves penetrate up to the ionosphere better at larger geomagnetic latitudes both because of magnetic inclination is closer to 90° and geomagnetic field is stronger.

[28] Comparison of the peak power spectral densities of Poynting fluxes of individual lines forming the PLHR events that were observed during the day and observed during the night reveals that the lines observed during the night are more intense than the lines observed during the day. The difference is 1.6 standard deviation, supposing that the lines forming one event are completely independent and 1.1 standard deviation, supposing that the lines forming one event can be considered as completely dependent. The real situation probably corresponds to something in between—the lines forming the same event are dependent, but only partially. The performed calculation of the efficiency of coupling of electromagnetic waves through the ionosphere seems to explain this difference completely—the estimated radiated peak power spectral density of Poynting flux corresponding to the events observed during the night is lower than during the day. The difference is statistically quite significant: 2.9 standard deviations and 1.9 standard deviation for completely independent/completely dependent lines forming one event, respectively. A possible explanation could be that during the day a power system is more loaded and the PLHR events are consequently stronger. This would also explain the larger number of PLHR events observed during the day than the night: in Figure 10 there are 43 events and 24 events, observed respectively during the day time and during the night time. Supposing a binomial distribution, this corresponds to about 2.3 standard deviations. Moreover, because of the larger efficiency of coupling even less intense events radiated during the nighttime are intense enough to be detected on board DEMETER.

[29] Finally, we can compare ground levels of estimated radiated Poynting fluxes based on DEMETER observations with the ones deduced from the ground measurements [*Bullough*, 1995, chapter 2.2]. Their estimates for Poynting fluxes at the base of the ionosphere (before the attenuation starts to take place) are in the range of $5.8 \cdot 10^{-10}$ nW m^{-2} (*Bullough* [1995], page 297, table 10.2.1, Cooks Harbour power line) up to $7.9 \cdot 10^{-4}$ nW m^{-2} (*Bullough* [1995], page 298, equation 2.9, Derbyshire Cement Works) in 1 kHz frequency band around 2.5 kHz. The estimated radiated Poynting fluxes of individual PLHR lines determined from DEMETER data are between $5.18 \cdot 10^{-7}$ nW m^{-2} and $5 \cdot 10^{-4}$ nW m^{-2} and we usually observe about three lines forming the PLHR event. One can see that the weakest lines detected on the ground are too weak to be detected on board DEMETER. However, our estimated values of Poynting flux are well within the range determined from ground-based measurements.

7. Conclusions

[30] Results of a systematic study of observations of PLHR by a low-altitude satellite have been presented. Altogether, 88 events (45 with frequency spacing 50/100 Hz and 43 with frequency spacing 60/120 Hz) have been found by an automatic identification procedure in about 3378 hours of Burst-mode data and statistically analyzed. For each of the individual lines forming the events, parameters of frequency-time-dependent 2d-Gaussian model have been found by an automatic procedure.

[31] Our results show that the mean FWHM of time duration of the observed lines is on average 20 seconds (median 12 seconds), which corresponds to average spatial dimensions of 156 km (median 90 km). The FWHM of the frequency range of individual lines is less than 3 Hz in the majority of cases. The most intense lines occur off exact multiples of base power system frequency. The lines with larger bandwidth usually occur off exact multiples of power system frequency as well. Full-wave calculation of efficiency of coupling of electromagnetic waves through the ionosphere has been done and it is shown that it can explain the lower intensity of PLHR events observed by satellite during the day as compared to those observed during the night. Estimated radiated peak power on the ground is larger for events observed during the day than for events observed during the night and more events are observed during the day than during the night.

[32] **Acknowledgments.** The authors thank J. J. Berthelier for the use of electric field data. We thank J.-Y. Brochot of LPCE/CNRS Orléans for his help with running the PLHR recognition algorithm as the DEMETER level-3 processing procedure. We thank SPDF/Modelweb for the free access to the data from the International Reference Ionosphere model. We thank M. Rycroft for useful discussion. F.N. and O.S. acknowledge support of the GACR grant 205/06/1267. F.N., O.S., and M.P. acknowledge support of the PICS grant 3725 from CNRS/DREI.

[33] Amitava Bhattacharjee thanks Mike Kosch and Michael Rycroft for their assistance in evaluating this paper.

References

Ando, Y., M. Hayakawa, and O. A. Molchanov (2002), Theoretical analysis on the penetration of power line harmonic radiation into the ionosphere, *Radio Sci.*, *37*(6), 1093, doi:10.1029/2001RS002486.

Bell, T. F., J. P. Luette, and U. S. Inan (1982), ISEE 1 observations of VLF line radiation in the earth's magnetosphere, *J. Geophys. Res.*, *87*(A5), 3530–3536.

Berthelier, J. J., et al. (2006), ICE, the electric field experiment on DEMETER, *Planet. Space Sci.*, *54*, 456–471.

Bilitza, D. (1990), *International Reference Ionosphere*, NSSDC 90-22, Greenbelt, Md.

Bortnik, J., and T. Bleier (2004), Full wave calculation of the source characteristics of seismogenic electromagnetic signals as observed at LEO satellite altitudes, *Eos Trans. AGU*, *85*(47), Fall Meet. Suppl., Abstract T51B-0453.

Bullough, K. (1995), Handbook of atmospheric electrodynamics, in *Power Line Harmonic Radiation: Sources and Environmental Effects*, vol. 2, edited by H. Volland, pp. 291–332, CRC Press, Boca Raton, Fla.

Cummer, S. A. (2000), Modeling electromagnetic propagation in the Earth-ionosphere waveguide, *IEEE Trans. Antennas Propag.*, *48*, 1420.

Helliwell, R. A. (1965), *Whistlers and Related Ionospheric Phenomena*, Stanford Univ. Press, Stanford, Calif.

Helliwell, R. A., J. P. Katsufrakis, T. F. Bell, and R. Raghuram (1975), VLF line radiation in the earth's magnetosphere and its association with power system radiation, *J. Geophys. Res.*, *80*(31), 4249–4258.

Karinen, A., K. Mursula, T. Ulich, and J. Manninen (2002), Does the magnetosphere behave differently on weekends?, *Ann. Geophys.*, *20*(8), 1137–1142.

Koons, H. C., M. H. Dazey, and B. C. Edgar (1978), Satellite observation of discrete VLF line radiation within transmitter-induced amplification bands, *J. Geophys. Res.*, *83*(A8), 3887–3889.

Manninen, J. (2005), Some aspects of ELF-VLF emissions in geophysical research, in *Power Line Harmonic Radiation*, pp. 53–84, 98, Sodankylä Geophysical Observatory Publications, Sodankylä, Finland.

Matthews, J. P., and K. Yearby (1981), Magnetospheric VLF line radiation observed at Halley, Antarctica, *Planet. Space Sci.*, *29*, 97–106.

Molchanov, O. A., M. Parrot, M. M. Mogilevsky, and F. Lefeuvre (1991), A theory of PLHR emissions to explain the weekly variation of ELF data observed by a low-altitude satellite, *Ann. Geophys.*, *9*, 669–680.

Nagano, I., M. Mambo, and G. Hutatsuishi (1975), Numerical calculation of electromagnetic waves in an anisotropic multilayered medium, *Radio Sci.*, *10*(6), 611–617.

Němec, F., O. Santolík, M. Parrot, and J. J. Berthelier (2006), Power line harmonic radiation (PLHR) observed by the DEMETER spacecraft, *J. Geophys. Res.*, *111*, A04308, doi:10.1029/2005JA011480.

Němec, F., O. Santolík, M. Parrot, and J. J. Berthelier (2007a), Comparison of magnetospheric line radiation and power line harmonic radiation: A systematic survey using the DEMETER spacecraft, *J. Geophys. Res.*, *112*, A04301, doi:10.1029/2006JA012134.

Němec, F., O. Santolík, M. Parrot, and J. J. Berthelier (2007b), Power line harmonic radiation: A systematic study using DEMETER spacecraft, *Adv. Space Res.*, *40*, 398–403.

Nunn, D., J. Manninen, T. Turunen, V. Trakhtengerts, and N. Erokhin (1999), On the nonlinear triggering of VLF emissions by power line harmonic radiation, *Ann. Geophys.*, *17*, 79–94.

Park, C. G., and R. A. Helliwell (1978), Magnetospheric effects of power line radiation, *Science*, *200*, 727–730.

Park, C. G., and R. A. Helliwell (1981), Power line radiation in the magnetosphere, *Adv. Space Res.*, *1*, 423–437.

Park, C. G., and R. A. Helliwell (1983), Ground observations of power line radiation coupled to the ionosphere and magnetosphere, *Space Sci. Rev.*, *35*, 131–137.

Park, C. G., and T. R. Miller (1979), Sunday decreases in magnetospheric VLF wave activity, *J. Geophys. Res.*, *84*(A3), 943–950.

Parrot, M., O. Molchanov, M. Mogilevski, and F. Lefeuvre (1991), Daily variations of ELF data observed by a low-altitude satellite, *Geophys. Res. Lett.*, *18*(6), 1039–1042.

Parrot, M., F. Němec, O. Santolík, and J. J. Berthelier (2005), ELF magnetospheric lines observed by DEMETER, *Ann. Geophys.*, *23*, 3301–3311.

Parrot, M., et al. (2006), The magnetic field experiment IMSC and its data processing onboard DEMETER: Scientific objectives, description and first results, *Planet. Space Sci.*, *54*, 441–455.

Parrot, M., J. Manninen, O. Santolík, F. Němec, T. Turunen, T. Raita, and E. Macúšová (2007), Simultaneous observation on board a satellite and on the ground of large-scale magnetospheric line radiation, *Geophys. Res. Lett.*, *34*, L19102, doi:10.1029/2007GL030630.

Rodger, C. J., N. R. Thomson, and R. L. Dowden (1995), VLF line radiation observed by satellite, *J. Geophys. Res.*, *100*(A4), 5681–5689.

Rodger, C. J., M. A. Clilverd, K. Yearby, and A. J. Smith (2000), Is magnetospheric line radiation man-made?, *J. Geophys. Res.*, *105*(A7), 15,981–15,990.

Santolík, O., F. Němec, M. Parrot, D. Lagoutte, L. Madrias, and J. J. Berthelier (2006), Analysis methods for multi-component wave measurements on board the DEMETER spacecraft, *Planet. Space Sci.*, *54*, 512–527.

Stix, T. H. (1992), Wave normal surfaces: Waves in a cold uniform plasma, in *Waves in Plasma*, edited by American Institute of Physics, pp. 1–46, Springer, New York.

Tomizawa, I., and T. Yoshino (1985), Power line radiation observed by the satellite, *J. Geomagn. Geoelectr.*, *37*, 309–327.

Yearby, K. H., A. J. Smith, and K. Bullough (1983), Power line harmonic radiation in Newfoundland, *J. Atmos. Terr. Phys.*, *45*, 409–419.

J. Bortnik, Department of Atmospheric and Oceanic Sciences, University of California Los Angeles, 405 Hilgard Avenue, Los Angeles, CA 90095, USA.

F. Němec and M. Parrot, Laboratorie de Physique et Chimie l'Environnement/CNRS, 3A Avenue de la Recherche Scientifique, 45071 Orléans Cedex 2, France. (frantisek.nemec@cnrs-orleans.fr)

O. Santolík, Institute of Atmospheric Physics/ASCR, Bocni II 1401, 141 31, Prague 4, Czech Republic.